

ARTICLE

Physiologically-Based Pharmacokinetic Model-Informed Drug Development for Fenebrutinib: Understanding Complex Drug-Drug Interactions

Yuan Chen^{1,*}, Fang Ma¹, Nicholas S. Jones², Kenta Yoshida³, Po-Chang Chiang⁴, Matthew R. Durk¹, Matthew R. Wright¹, Jin Yan Jin³ and Leslie W. Chinn³

Fenebrutinib is a CYP3A substrate and time-dependent inhibitor, as well as a BCRP and OATP1B transporter inhibitor *in vitro*. Physiologically-based pharmacokinetic (PBPK) modeling strategies with the ultimate goal of understanding complex drug-drug interactions (DDIs) and proposing doses for untested scenarios were developed. The consistency in the results of two independent approaches, PBPK simulation and endogenous biomarker measurement, supported that the observed transporter DDI is primarily due to fenebrutinib inhibition of intestinal BCRP, rather than hepatic OATP1B. A mechanistic-absorption model accounting for the effects of excipient complexation with fenebrutinib was used to rationalize the unexpected observation of itraconazole-fenebrutinib DDI (maximum plasma concentration (C_{max}) decreased, and area under the curve (AUC) increased). The totality of the evidence from sensitivity analysis and clinical and nonclinical data suggested that fenebrutinib is likely a sensitive CYP3A substrate. This advanced PBPK application allowed the use of model-informed approach to facilitate the development of concomitant medication recommendations for fenebrutinib without requiring additional clinical DDI studies.

Study Highlights

WHAT IS THE CURRENT KNOWLEDGE ON THE TOPIC?

☑ Model-informed drug development (MIDD) has become an important approach to improve clinical trial efficiency, optimize drug dosing, and propose drug labeling in the absence of dedicated trials. Experiences from PBPK MIDD for drugs with complex drug-drug interactions are desired to build up confidence in using the approach and increase the probability of regulatory success.

WHAT QUESTION DID THIS STUDY ADDRESS?

☑ Can we use PBPK mechanistic modeling strategy with incorporation of nonclinical (e.g., drug-excipient complexation effect) data, and in combination with clinical (e.g., endogenous biomarker) data to rationalize clinical observation of complex DDI results and ultimately use PBPK MIDD to inform the comedication strategy in example with fenebrutinib?

WHAT DOES THIS STUDY ADD TO OUR KNOWLEDGE?

☑ The study indicates that fenebrutinib-excipient complexation is the cause of an unexpected result of DDI between itraconazole and fenebrutinib, and the totality of

evidences from PBPK simulation and other clinical studies suggest that fenebrutinib is likely a sensitive CYP3A4 substrate. It also suggests that the transporter inhibition DDI caused by fenebrutinib is mainly due to its inhibition in gut BCRP rather than hepatic OATP1B.

HOW MIGHT THIS CHANGE DRUG DISCOVERY, DEVELOPMENT, AND/OR THERAPEUTICS?

☑ This study uncovered an important role of physical drug-excipient complexation and how it can affect interpretation of metabolic DDIs observed in clinical studies. The mechanistic PBPK absorption model with incorporation of drug-excipient complexation effect can explain confounding DDI results between a CYP3A substrate (i.e., fenebrutinib) and a strong inhibitor (i.e., itraconazole), and ultimately confirm the $f_{m,CYP3A4}$ without conducting additional dedicated DDI studies. The combined PBPK modeling and endogenous biomarker approach can be used to increase our confidence in understanding clinical DDI involving multiple transporters. This work has provided an example of the PBPK model-informed drug development approach.

¹Department of Drug Metabolism and Pharmacokinetics, Genentech, Inc., South San Francisco, California, USA; ²Department of Clinical Science, Genentech, Inc., South San Francisco, California, USA; ³Department of Clinical Pharmacology, Genentech, Inc., South San Francisco, California, USA; ⁴Department of Pharmaceutical Science, Genentech, Inc., South San Francisco, California, USA. *Correspondence: Yuan Chen (chen.yuan@gene.com)

Received: January 23, 2020; accepted: March 30, 2020. doi:10.1002/psp4.12515

Fenebrutinib, an orally administered, potent, and selective reversible antagonist of Bruton's tyrosine kinase is being developed as a potential therapy for autoimmune diseases.¹ Phase I clinical studies have been conducted to characterize fenebrutinib disposition in humans.² The *in vitro* data indicated that fenebrutinib is both a substrate and a time-dependent inhibitor of cytochrome P450 3A (CYP3A). Fenebrutinib also inhibits organic-anion-transporting polypeptides (OATP1B1/3), breast cancer resistance protein (BCRP), and P-glycoprotein (P-gp) transporters.³ To assess the clinical drug-drug interaction (DDI) risk, a physiologically-based pharmacokinetic (PBPK) model was developed to predict the magnitude of DDI between fenebrutinib and CYP3A substrates (midazolam and simvastatin), fenebrutinib and a BCRP and OATP1B substrate (rosuvastatin), and fenebrutinib and strong CYP3A inhibitor (itraconazole). Although these prospective PBPK simulations predicted the clinically observed DDI (i.e., fenebrutinib as an inhibitor of CYP3A and transporter substrates), a further mechanistic understanding of the unexpected effect of itraconazole on fenebrutinib pharmacokinetics (PKs), as well as the DDI caused by fenebrutinib BCRP and OATP1B transporter inhibition is required in order to use the model to predict untested scenarios and inform labeling.

Prospective PBPK simulations predicted increases in both fenebrutinib maximum plasma concentration (C_{max}) and area under the curve (AUC) in the presence of itraconazole, however, in the DDI study, while multiple doses of 200 mg itraconazole solution increased fenebrutinib AUC, there was an unexpected decrease in C_{max} and a delay in time to reach the C_{max} (T_{max}). Understanding the cause of clinical observation using mechanistic modeling with a hypothesis supported by *in vitro* and *in vivo* data is ultimately important to determine CYP3A contribution ($f_{m,CYP3A}$) to fenebrutinib clearance, and subsequently the DDI between fenebrutinib and other CYP3A inhibitors.

In the clinical DDI study between fenebrutinib and rosuvastatin, increase in rosuvastatin exposure in the presence of fenebrutinib was observed, and, as expected from prospective PBPK simulations, the increase in rosuvastatin C_{max} was larger than AUC, likely due to stronger inhibition of BCRP compared with OATP1B by fenebrutinib. Confirmation of the relative contribution of OATP1B vs. BCRP inhibition by fenebrutinib to the total observed DDI using PBPK simulation and other clinical data is desired in order to increase confidence in predicting fenebrutinib DDI with other OATP1B substrates that may be co-administered with fenebrutinib.

Here, we present two integrated approaches to support PBPK model-informed fenebrutinib drug development: (i) using a mechanistic absorption PBPK model, incorporating the effect of excipient from itraconazole solution (i.e., hydroxypropyl- β -cyclodextrin (H- β -CD)-fenebrutinib complexation), to rationalize the observed clinical DDI between itraconazole and fenebrutinib, and thereafter determine fenebrutinib $f_{m,CYP3A}$ through retrospective simulations and verification using additional clinical data; and (ii) using combined PBPK simulations and endogenous biomarker measurements for a better mechanistic understanding of a clinical DDI (i.e., between fenebrutinib and rosuvastatin) involving multiple transporters. Ultimately, with increased

confidence through better mechanistic understanding, these PBPK model-based approaches may facilitate development of clinical recommendations around concomitant medication use for fenebrutinib, without requiring additional clinical DDI studies.

METHODS

Preclinical *in vitro* and *in vivo* data

In vitro studies³ to assess fenebrutinib as CYP3A substrate, transporter, and CYP3A enzyme inhibitor are presented in the **Supplementary Material**.

To evaluate the complexation interaction between fenebrutinib and H- β -CD, an excipient in itraconazole solution, the *in vitro* experiments were conducted using a Madin-Darby Canine Kidney (MDCK) cell monolayer system, and the effect on apparent fenebrutinib permeability (P_{app}) at various concentrations of H- β -CD were measured. Moreover, PK study in pentagastrin-pretreated dogs with fenebrutinib tablets administered orally, with and without H- β -CD, was conducted, and the effect of H- β -CD on fenebrutinib absorption was assessed. Details of these studies are described elsewhere (manuscript in preparation).

Clinical DDI study

A phase I DDI study³ was conducted in healthy subjects to evaluate the effect of fenebrutinib on the PKs of midazolam, rosuvastatin, and simvastatin; and the effect of itraconazole on the PK of fenebrutinib (**Supplementary Material**).

Fenebrutinib PBPK model

The overall PBPK modeling strategy is presented in **Figure 1**. The fenebrutinib model was built using *in vitro* and preclinical absorption, distribution, metabolism, elimination (ADME) data, and further refined and verified based on phase I PK data. The prospective DDI simulations for fenebrutinib as a CYP3A substrate and inhibitor, and an OATP1B and BCRP transporter inhibitor were conducted prior to clinical DDI study. As the clinical DDI data became available, retrospective mechanistic PBPK analysis was conducted to verify the assumptions used in the prediction and rationalize the unexpected clinical observations.

The Simcyp Population-based ADME Simulator (version 16; Sheffield, UK) with a healthy volunteer population ("Sim – Healthy Volunteers") was used to build the fenebrutinib PBPK model. Models describing fenebrutinib absorption, distribution, and elimination are summarized below:

Absorption: The Advanced Dissolution, Absorption, and Metabolism (ADAM) model was used to describe the absorption of fenebrutinib tablet. The cumulative absorption was predicted based on measured pH-solubility data and dissolution profile predicted by the model. The human jejunum effective permeability ($P_{eff,man}$) was predicted from measured MDCK data (**Table 1**). **Distribution:** Volume of distribution at steady-state (V_{ss}) was predicted using tissue composition equations⁴ in the model. The Simcyp minimal PBPK (which treats all organs other than the intestine and liver as a single

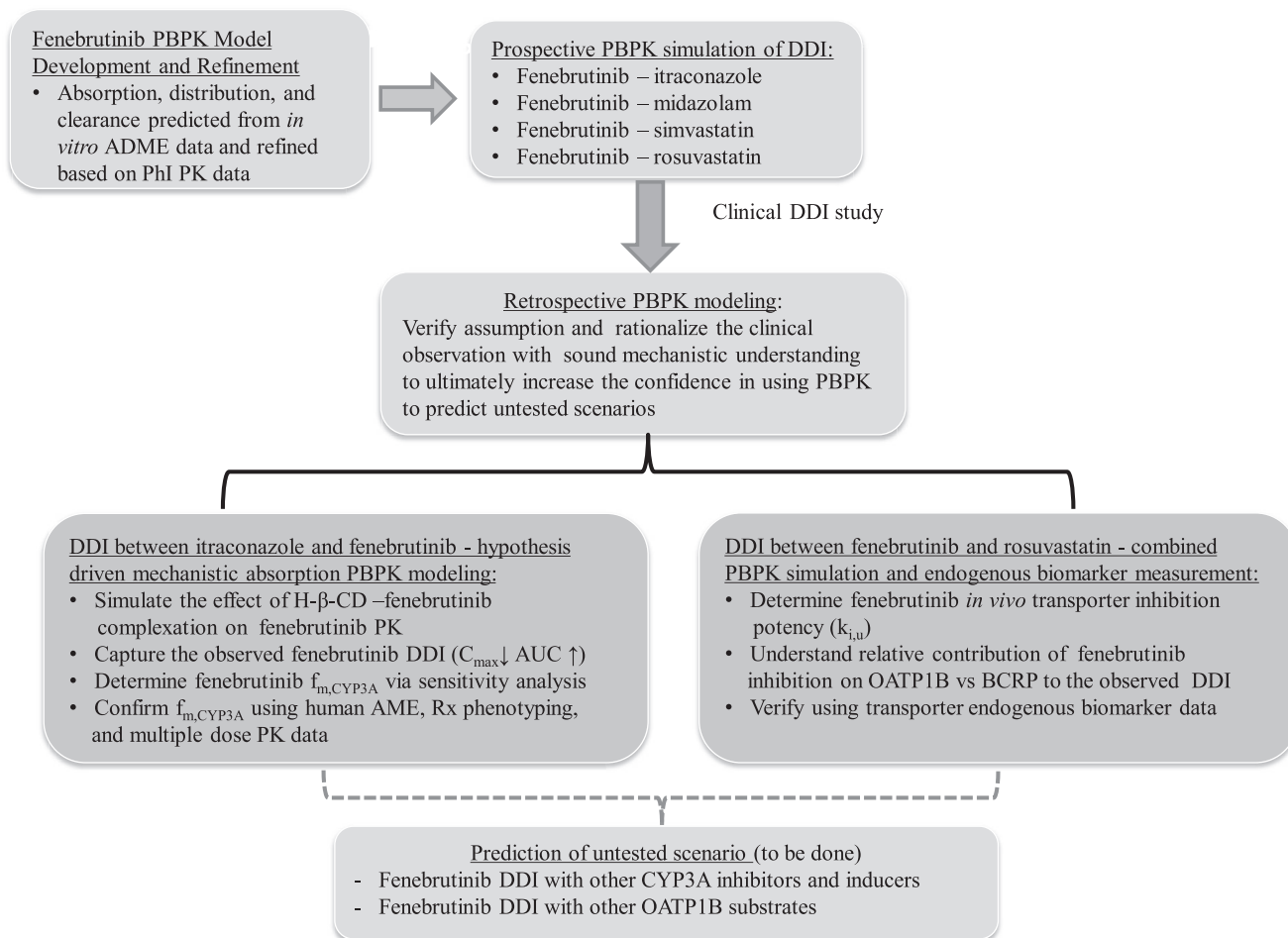


Figure 1 Overall physiologically-based pharmacokinetic (PBPK) model-informed fenebrutinib development strategy. ADME, absorption, distribution, metabolism, elimination; AME, absorption, metabolism, and excretion; AUC, area under the concentration-time curve; BCRP, breast cancer resistance protein; C_{max} , maximum plasma concentration; DDI, drug-drug interaction; $f_{m,CYP3A}$, contribution of CYP3A to fenebrutinib clearance; $K_{i,u}$, unbound transporter inhibition constant; OATP, organic anion-transporting polypeptide; PKs, pharmacokinetics.

compartment⁵ plus a single adjusting compartment (SAC) distribution model was selected to best describe the multiphasic fenebrutinib PK profile. Final values of apparent volume of SAC, rate constant from systemic compartment to SAC (K_{in}), and rate constant from SAC to the systemic compartment (K_{out}) were determined from simulations that best describe the shape of the observed PK profile.

Elimination: Preclinical data indicated hepatic metabolism predominantly through CYP3A4 as the main clearance pathway for fenebrutinib. Therefore, in the fenebrutinib elimination model, the total clearance (CL) estimated based on phase I PK was assigned to major hepatic clearance primarily through CYP3A4 and minor renal clearance.

Simulations of fenebrutinib PK were performed using 10 virtual trials of 10 healthy volunteers per trial, aged 20–50 years, and a 1:1 female-to-male ratio. In phase I PK studies, fenebrutinib was administered as solution, capsule (single and multiple-day dose),² and tablet (200 mg

relative bioavailability study; unpublished data) dosage forms. Because the DDI studies used tablet form, the PBPK absorption model was developed to describe PK of fenebrutinib tablet, and model's performance was evaluated by overlaying the simulated mean concentration-time profiles with clinical data.

Prospective simulation of fenebrutinib DDI

To assess DDI risk for fenebrutinib as CYP3A substrate or inhibitor, or BCRP and OATP1B1/3 transporter inhibitor, PBPK simulations were conducted prior to DDI studies to predict the magnitude of DDI between itraconazole and fenebrutinib, fenebrutinib and midazolam, fenebrutinib and simvastatin, and fenebrutinib and rosuvastatin. The default PBPK models for midazolam, simvastatin, and rosuvastatin available in Simcyp (version 16) compound library were used. The itraconazole and its metabolite hydroxy-itraconazole models in Simcyp compound library were modified based on our previous work.⁶ Key parameters for rosuvastatin and itraconazole are presented in **Tables S1 and S2**.

Table 1 Key parameters for final fenebrutinib PBPK model

Parameters	Value	Methods/references
MW	664.8	
logP	3.3	Measured
pK_{a1} , pK_{a2}	5, 3.7	Diprotic base
$f_{u,p}$	0.197	Measured
B/P	0.61	Measured
Absorption	ADAM absorption model	
MDCK, 10^{-6} cm/s	15.1	Measured
$P_{\text{eff-man}}$, 10^{-4} cm/s	7.56	Simcyp predicted using MDCK- P_{app} with scalar of 3.9 calculated from references (Model 1)
$P_{\text{eff-man}}$, 10^{-4} cm/s Duodenum/jejunum I/jejunum II/ileum I/ ileum II/ileum III/ileum IV/colon	0.088/0.22/0.15/1.13/1.13/1.1/ .1/0.588	Simcyp Mech P_{eff} model predicted regional P_{eff} with manually reduced P_{eff} (30x) in duodenum, jejunum I, and jejunum II (Model 2)
pH solubility profile 2.3/2.6/3.0/3.8/5.0/ 6.1/6.9/7.7/9.2	35.9/5.67/1.44/0.032/0.001/0. 001.....	Measured
CSR	100	Best fit
PRC, 1/hour	1	Best fit
Dissolution	Predicted	Based on <i>in vitro</i> biopharmaceutical data (solubility, permeability, FaSSIF and FeSSIF, particle size)
Log $K_{m,w}$ neutral	5.35	Model calculated based on measured FaSSIF and FeSSIF
Distribution	Minimal + SAC PBPK model	
V_{ss} , L/kg	5.23	Simcyp method 2 (Rodgers and Rowland, 2006), K_p scalar 0.315
V_{sac} , L/kg	3.25	Best fit
K_{in}/K_{out} , 1/hour	0.015/0.05	Best fit
Elimination	Enzyme kinetics (Recombinant)	
$CL_{\text{int-CYP3A4}}$, pmol/min/pmol of isoform	0.4/0.51/0.64/0.695/0.74/0.82	Corresponding to $f_{m,CYP3A4}$ of 0.5/0.6/0.75/0.8/0.85/0.9, account for 50 /60/75/80/85/90% of total CL
Additional liver $CL_{\text{int-hep}}$, $\mu\text{L}/\text{min}/10^6$	17.5/12.5/07.1/5.5/4.4/2.4	
CL_{Renal} , L/hour	1.1	Account for ~ 5% of total CL, based on human AME data
CYP inhibition		
CYP3A TDI K_i/K_{inact} , μM , 1/hour	7.9/0.684	Measured
$f_{u,mic}$	0.5	Optimized to best capture observed DDI (Simcyp model predicted to be 0.97)
Transporter inhibition		
$K_{i,u}$ -OATP1B1, μM	0.1379	Measured $IC_{50}/2*0.014$ (lumped scaling factor)
$K_{i,u}$ -OATP1B3, μM	0.05005	
$K_{i,u}$ -BCRP, μM	0.0658	
$K_{i,u}$ -P-gp, μM	0.2121	

ADAM, advanced dissolution, absorption, and metabolism; BCRP, breast cancer resistance protein; B/P ratio, blood/plasma partition ratio; CL, clearance; CL_{int} , intrinsic clearance; CSR, critical supersaturation ratio; f_a , fraction absorbed; FaSSIF, fasted state simulated intestinal fluid; FeSSIF, fed state simulated intestinal fluid; $f_{u,mic}$, free fraction in liver microsome; $f_{u,p}$, free fraction in plasma; IC_{50} , half-maximal inhibitory concentration; k_a , absorption rate constant; K_i , concentration at 50% of K_{inact} ; $K_{i,u}$, unbound transporter inhibition constant; k_{in} , rate constant from systemic compartment to SAC; K_{inact} , maximum enzyme inactivation; k_{out} , rate constant from SAC compartment to the systemic compartment; Log $K_{m,w}$, logarithm of bile micelle: buffer partition coefficients; LogP, octanol-water partition co-efficient; MW, molecular weight; OATP, organic anion-transporting polypeptide; P_{app} , apparent fenebrutinib permeability; PBPK, physiologically-based pharmacokinetics; P_{eff} , effective permeability; $P_{\text{eff-man}}$, human jejunum effective permeability; P-gp, P-glycoprotein; PRC, precipitation rate constant; pK_a , acid dissociation constant; V_{sac} , volume of the single adjusted compartment; V_{ss} , volume of distribution at steady state.

To predict DDI with fenebrutinib as perpetrator, fenebrutinib *in vitro* time-dependent CYP3A inhibition kinetic data (K_i , concentration at 50% of K_{inact} and K_{inact} , maximum enzyme inactivation), and transporter inhibition K_i (inhibition constant) for OATP1B1/3 and BCRP were entered into the fenebrutinib model. For fenebrutinib as a victim, in prospective simulation of DDI between itraconazole and fenebrutinib, 3 scenarios with f_{mCYP3A} as 50%, 75%, and 90% were simulated because the f_{mCYP3A} of fenebrutinib could not be confirmed solely based on *in vitro* data before clinical DDI and human mass balance study data became available.

The simulations were performed using a Simcyp virtual population, as described earlier.

Retrospective PBPK analysis for mechanistic understanding of complex DDI

After clinical DDI study data became available, retrospective PBPK simulations were conducted to rationalize clinical observation and further refine the model with better mechanistic understanding before applying the model to simulate DDI to inform fenebrutinib concomitant medication strategy.

The overall approach of retrospective PBPK analysis (**Figure 1**) includes: (i) using mechanistic absorption model incorporating hypothesized H- β -CD excipient effect to explain the unexpected change in fenebrutinib PK when co-administered with itraconazole, and determining and verifying $f_{m,CYP3A}$ in fenebrutinib clearance using all existing clinical data; and (ii) performing sensitivity analysis on fenebrutinib OATP1B1/3 and BCRP inhibition $K_{i,u}$ (unbound K_i), and scenario simulations of fenebrutinib-rosuvastatin DDI to understand the relative contribution of fenebrutinib inhibition on OATP1B vs. BCRP to the observed DDI and verification using endogenous transporter biomarker data.

RESULTS

Preclinical *in vitro* and *in vivo* data

Fenebrutinib inhibited the OATP1B1 and OATP1B3-mediated uptake (half-maximal inhibitory concentration (IC_{50}) 19.7 μ M and 7.15 μ M, respectively); BCRP-mediated efflux (IC_{50} 9.40 μ M), and CYP3A enzyme (k_{inact} and apparent K_i of 0.0114 min^{-1} and 7.9 μ M, respectively). *In vitro* reaction phenotyping study indicated that CYP3A is the major enzyme responsible for the metabolism of fenebrutinib.

Fenebrutinib P_{app} decreased in the presence of H- β -CD in a concentration-dependent manner in the MDCK assay. At the molar ratio of H- β -CD (8 g) to fenebrutinib (100 mg) estimated in the DDI study (46:1) in which itraconazole solution was administered, an \sim 15-fold decrease in fenebrutinib P_{app} was observed, relative to that without H- β -CD. Results from a dog PK study indicated that upon co-administration, the apparent rate and extent of fenebrutinib absorption were substantially decreased in the presence of H- β -CD (manuscript in preparation).

Fenebrutinib PBPK model

The final fenebrutinib PBPK model parameters are shown in **Table 1**. A scalar of tissue plasma partition coefficient (K_p) of 0.3 was applied to match the predicted V_{ss} with the observed value estimated based on phase I PK data ($V_{ss}/F \sim$ 13.4 L/kg). Total clearance estimated from phase I PK data ($CL/F \sim$ 80 L/hour) was assigned to hepatic (\sim 95%) and renal clearance (\sim 5%) in the model describing fenebrutinib elimination. This initial assumption

of hepatic metabolism playing a predominant role in fenebrutinib elimination was confirmed later by human mass balance study results. The hepatic clearance was further assigned to CYP3A pathway with the input of intrinsic CYP3A clearance ($CL_{int-CYP3A}$) that will result in a $f_{m,CYP3A}$ of 50–90% of CL (**Table 1**). **Figure 2** shows the observed and simulated mean plasma concentration-time profiles of fenebrutinib (200 mg tablet) in the fasted and fed states. The ADAM model described the observed PK after oral administration; and the mini-PBPK distribution model captured the multi-exponential disposition PK profile of fenebrutinib.

Prediction of fenebrutinib DDI

For fenebrutinib as victim, the prospective simulation predicted increases in both C_{max} and AUC of fenebrutinib when co-administered with itraconazole. In the range of assumed $f_{m,CYP3A}$ from 0.5–0.9 (unknown in the prospective DDI simulation), the fenebrutinib AUC was predicted to increase by 2.2 to 9.3-fold and C_{max} by 1.6 to 2.8-fold, and no change in T_{max} , in the presence of itraconazole. However, in the clinical DDI study, multiple doses of 200 mg itraconazole solution (once daily \times 8 days) resulted in an increase in fenebrutinib AUC_{0-t} (AUC over the dosing interval, 2.28-fold) and, unexpectedly, a decrease in C_{max} (\sim 11%) and a delay in T_{max} (**Figure S1**).

To predict DDI in which fenebrutinib is a CYP3A time-dependent inhibitor, the *in vitro* K_i (7.9 μ M), K_{inact} (0.684 $hour^{-1}$), and $f_{u,mic}$ (unbound fraction in microsomal incubation, 0.97 to correct K_i) were entered into the fenebrutinib model. **Table 2** showed the comparisons of predicted vs. observed DDI between fenebrutinib and midazolam, and fenebrutinib and simvastatin. In the clinical DDI study, multiple doses of fenebrutinib affected the PK of midazolam and simvastatin, with a C_{max} and AUC ratios of 1.74 and 1.99 for midazolam, respectively, and 1.93 and 2.48 for simvastatin, respectively.³ The predicted DDI is within 1.5-fold of the observed data for both midazolam and simvastatin, with a trend of underprediction. The $f_{u,mic}$ (0.97) used in prospective simulation was predicted⁷ because there were no experimental data available. Retrospectively, when the $f_{u,mic}$ value adjusted from 0.97 to 0.5, the model

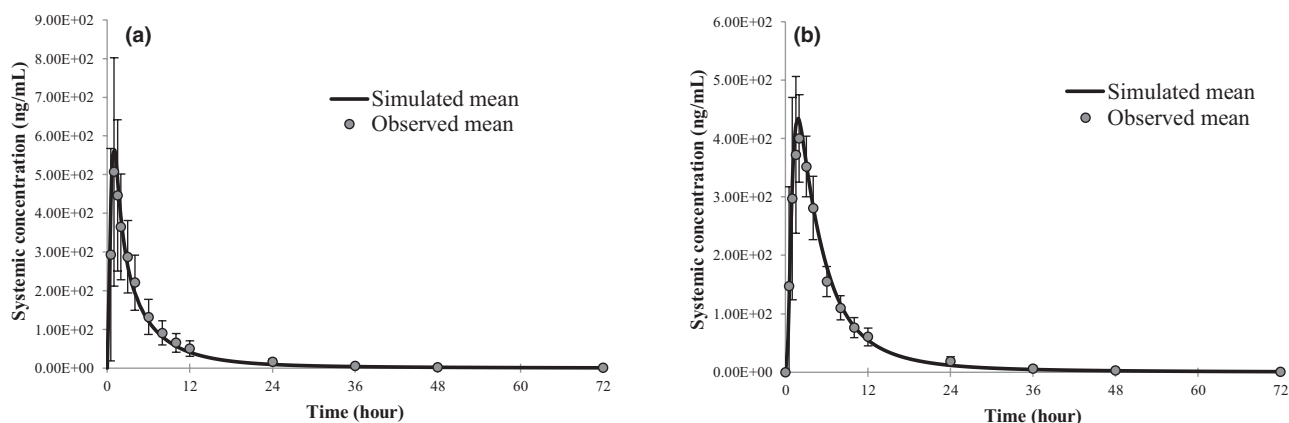


Figure 2 Observed and simulated plasma concentration-time profiles of fenebrutinib after oral administration of fenebrutinib. (a) Administered 200 mg tablet under fasted and (b) 200 mg under fed state in healthy subjects.

Table 2 Predicted vs. observed DDI for fenebrutinib as a CYP3A enzyme and OATP1B and BCRP transporter inhibitor

	Prospective simulation		Retrospective simulation		Observed	
	$C_{\max}R$	AUCR	$C_{\max}R$	AUCR	$C_{\max}R$	AUCR
Fenebrutinib as CYP3A TDI						
200 mg b.i.d. × 8 days, midazolam (2 mg) on day 7	1.28 (1.25–1.31)	1.57 (1.48–1.66)	1.49 (1.44–1.54)	2.18 (1.97–2.42)	1.74 (1.58–1.91)	1.99 (1.80–2.22)
200 mg b.i.d. × 8 days, simvastatin (40 mg) on day 7	1.59 (1.53–1.65)	1.78 (1.68–1.88)	2.17 (2.03–2.31)	2.68 (2.43–2.97)	1.93 (1.63–2.28)	2.48 (2.01–3.07)
Fenebrutinib as OATP1B1/3 and BCRP inhibitor						
200 mg b.i.d. × 10 days, rosuvastatin on day 7	1.95 (1.85–2.06)	1.10 (1.10–1.11)	5.08 (4.84–5.34)	1.63 (1.58–1.68)	4.99 (3.90–6.40)	2.66 (2.37–2.98)
200 mg b.i.d. × 10 days, rosuvastatin on day 7 (scenario simulation-no BCRP inhibition)			1.56 (1.50–1.62)	1.36 (1.32–1.40)		

AUCR, area under the curve ratio (geometric mean, 90% confidence interval); $C_{\max}R$, maximum plasma concentration ratio (geometric mean, 90% confidence interval); DDI, drug-drug interaction; TDI, time-dependent inhibitor.

simulations could more closely capture the observed DDI for both midazolam and simvastatin (Table 2).

To predict transporter DDI, the fenebrutinib transporter inhibition $K_{i,u}$ values (BCRP = 0.926 μM , OATP1B1 = 1.94 μM , and OATP1B3 = 0.704 μM) were entered into the PBPK model under gut and liver transporter interaction. The inhibition $K_{i,u}$ was estimated using *in vitro* measured $IC_{50}/2$ and then corrected by $f_{u,p}$ (unbound fraction in plasma) because no measured value of unbound fraction in transporter incubation ($f_{u,inc}$) is available. Table 2 showed the comparisons of predicted vs. observed DDI between fenebrutinib and rosuvastatin. In the clinical DDI study, multiple doses of fenebrutinib (200 mg twice daily dose for 10 days) affected the PK of rosuvastatin, with C_{\max} and AUC_{0-t} increasing by ~ 5-fold and 2.6-fold, respectively.³ While the prospective DDI simulation captured the trend in the observed DDI data, increase in C_{\max} was about twice that of AUC, the absolute magnitude of the DDI was underpredicted by ~ 2-fold.

Retrospective PBPK analysis for mechanistic understanding of complex DDI

Itraconazole–fenebrutinib DDI. To understand the unexpected decrease in fenebrutinib C_{\max} in the presence of itraconazole, the effect of complexation between fenebrutinib and H- β -CD on the absorption of fenebrutinib was considered. Data from the *in vitro* permeability experiment and an *in vivo* dog PK study supported the hypothesis that, in the presence of H- β -CD, formation of fenebrutinib-H- β -CD complex could result in less amount of free fenebrutinib available permeating the intestinal membrane, and subsequently decreasing the absorption in the upper gastrointestinal (GI) tract.⁸

Therefore, to retrospectively simulate the DDI between fenebrutinib and itraconazole in the presence of H- β -CD, two absorption models were used: model 1 to simulate fenebrutinib PK dose alone (without H- β -CD effect) and model 2 to simulate fenebrutinib co-administered with itraconazole (with H- β -CD effect). Model 1 has the ADAM absorption model with a lumped P_{eff} predicted from MDCK permeability data (previously described in the Methods section),

whereas model 2 has the ADAM absorption model with GI regional P_{eff} predicted from mechanistic permeability module (MechPeff), and the regional P_{eff} at the upper GI tract (duodenum, jejunum I, and jejunum II) was manually reduced to mimic the effect of H- β -CD–fenebrutinib complexation on fenebrutinib absorption. All other model parameters are the same between two models (Table 1).

The simulated DDI with and without H- β -CD effect showed that the increase in fenebrutinib C_{\max} caused by itraconazole CYP3A inhibition can be offset by the reduced absorption of fenebrutinib due to H- β -CD–fenebrutinib complexation (Figure 3a,c). The observed net changes to fenebrutinib C_{\max} (11% decrease) and AUC (~ 2.3-fold increase) in the presence of itraconazole depend on both the extent of H- β -CD effect on fenebrutinib absorption and the magnitude of itraconazole CYP3A inhibition in the gut and liver for fenebrutinib, and the extent of latter is determined by the contribution of CYP3A ($f_{m,CYP3A}$) in fenebrutinib clearance. Therefore, the sensitivity analysis on $f_{m,CYP3A}$ values (0.5–0.95) in the presence and absence of itraconazole, with and without consideration of the H- β -CD effect was performed. As shown in Table 3, without considering the H- β -CD effect, none of the DDI simulations with fenebrutinib $f_{m,CYP3A}$ ranging from 0.5–0.95 was able to capture both the observed C_{\max} and AUC changes correctly. If the H- β -CD effect was not accounted for, at $f_{m,CYP3A}$ 0.5–0.6, the model simulation could capture the observed AUC ratio (AUCR) but overpredicted the C_{\max} ratio ($C_{\max}R$). On the other hand, simulations with consideration of H- β -CD effect was able to capture both C_{\max} and AUC changes at a fenebrutinib $f_{m,CYP3A}$ value of 0.8–0.85 (Table 3, Figure 3). Furthermore, a sensitivity analysis of the extent of H- β -CD effect with regard to the fenebrutinib $f_{m,CYP3A}$ value and the $C_{\max}R$ and AUCR in the presence of itraconazole was conducted. In a range of P_{eff} reduction (caused by H- β -CD effect) from 0–100-fold at a given $f_{m,CYP3A}$ ranging from 0.5–0.95, the observed $C_{\max}R$ and AUCR were both closely captured only at the $f_{m,CYP3A}$ of ~ 0.8–0.85 (Figure 4).

Finally, the $f_{m,CYP3A}$ 0.8–0.85 determined from PBPK simulation of the observed DDI with consideration of H- β -CD effect was further confirmed using other clinical data. Based

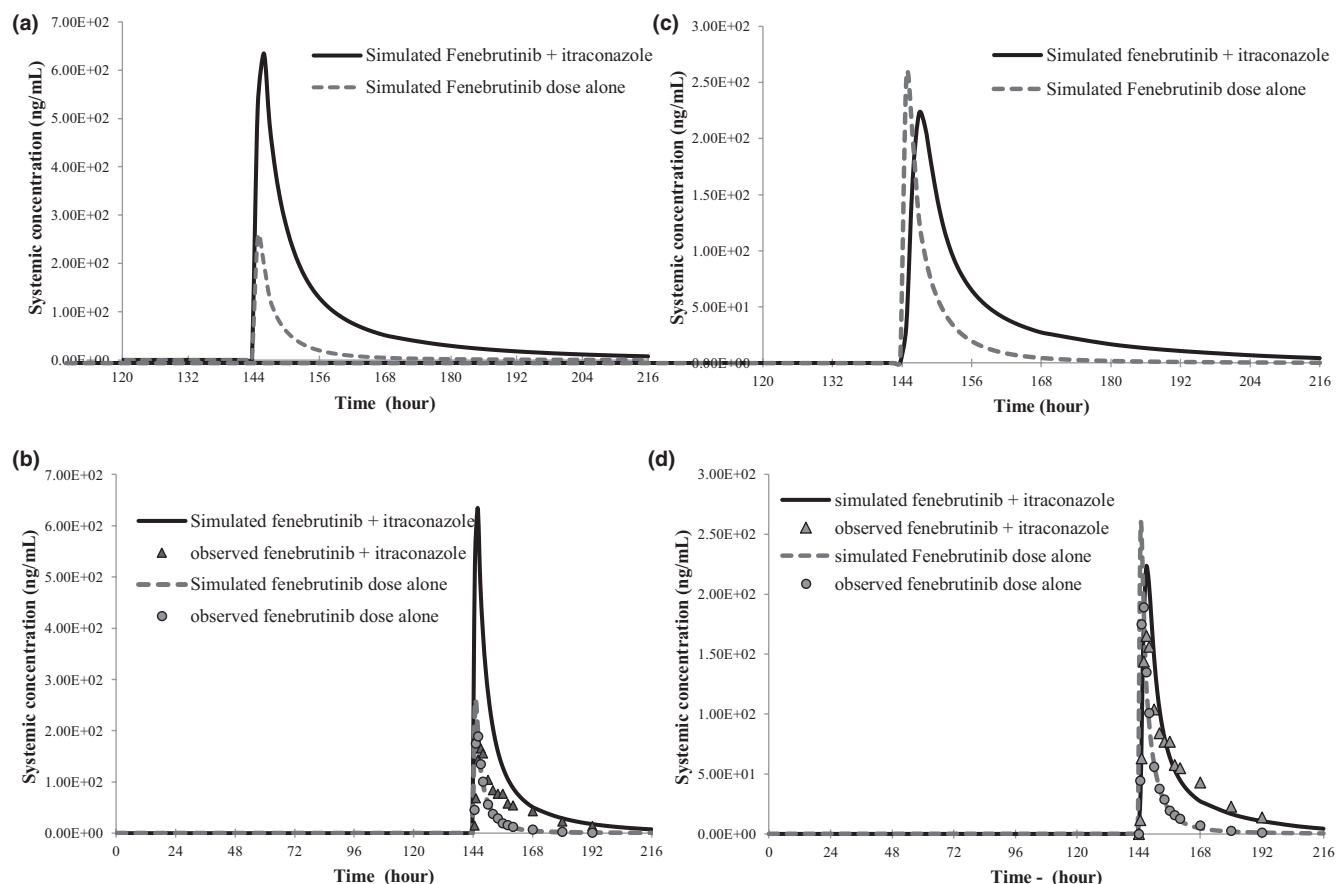


Figure 3 Observed and simulated fenebrutinib (100 mg tablet, on day 7) pharmacokinetics in the presence and absence of CYP3A inhibitor itraconazole (200 mg solution, q.d. × 8 day). (a, b) No consideration of H-β-CD effect; (c, d) with consideration of H-β-CD effect.

Table 3 Simulated fenebrutinib $C_{max}R$ and AUCR in the presence and absence of itraconazole and with and without consideration of H-β-CD effect

Fenebrutinib $f_{m,CYP3A}$	Without H-β-CD effect		With H-β-CD effect	
	$C_{max}R$	AUC _(0-T) R	$C_{max}R$	AUC _(0-T) R
0.5	1.57	2.06		
0.6	1.82	2.72	0.62	1.25
0.75	2.19	4.10	0.79	1.80
0.8	2.36	4.90	0.88	2.12
0.85	2.51	5.65	0.95	2.45
0.95	3.22	11.4	1.03	3.36
Observed	0.89	2.28	0.89	2.28

$C_{max}R$, maximum plasma concentration ratio (geometric mean); AUCR, area under the curve ratio (geometric mean)

on the human mass balance study (data available post-DDI study), fenebrutinib is eliminated predominantly (> 90%) through metabolic pathway with oxidative related metabolites accounting for ~ 80% of CL. *In vitro* phenotyping study revealed that CYP3A enzyme is predominantly responsible for oxidative metabolite formation. In addition, because

fenebrutinib is a CYP3A substrate as well as a time-dependent CYP3A inhibitor, some degree of auto-inhibition (and subsequent accumulation) could occur after multiple doses of fenebrutinib (based on PK terminal half-life at steady-state, accumulation is not expected).² As demonstrated by the PBPK simulations (Figure S2) as compared with the clinical PK data (200 mg b.i.d. × 10 days), the observed accumulation of fenebrutinib can be closely captured by the model at fenebrutinib $f_{m,CYP3A4}$ value of 0.8–0.85.

Fenebrutinib – rosuvastatin DDI. Retrospective analyses were conducted to understand the impact of $K_{i,u}$ on the predicted DDI. Although the trend of the observed DDI (i.e., $C_{max}R > AUCR$) was captured in the prospective model simulation, the magnitude of DDI was underpredicted by ~ 2-fold. In the prospective simulation of fenebrutinib transporter DDI, the $K_{i,u}$ for both BCRP and OATP1B1/3 were calculated using $f_{u,inc} = f_{u,p}$ (0.197) because there is no experimentally measured $f_{u,inc}$ value available. Retrospectively, the sensitivity analysis indicated that when the $K_{i,u}$ values for BCRP and OATP1B are ~ 15× lower than that used in the prospective model, or a lumped scaling factor of 0.014 was applied, the simulated DDI can more accurately capture the observed data (Table 2). The trend of underprediction of AUC in the retrospective analysis

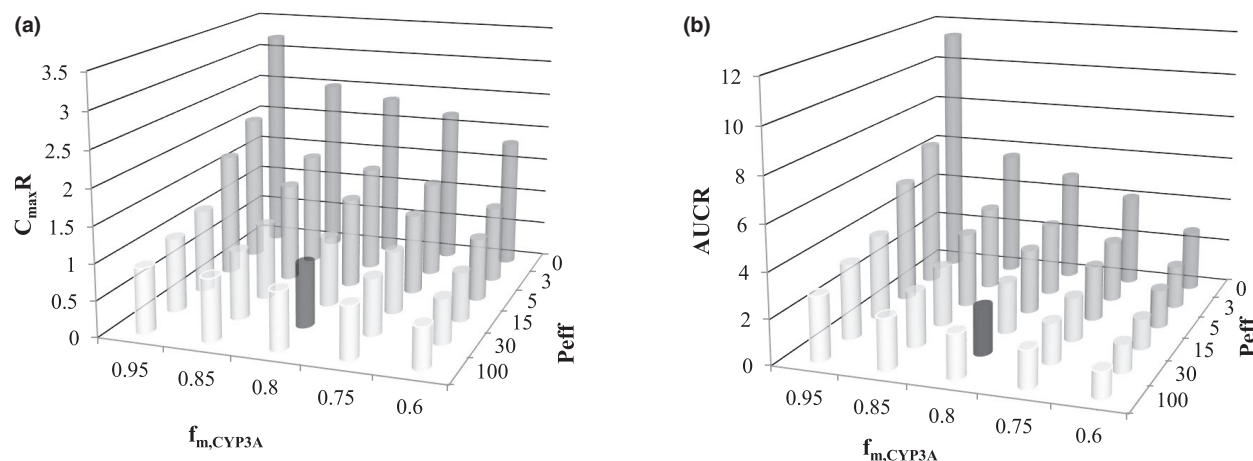


Figure 4 Sensitivity analysis of $f_{m,CYP3A}$ and the extent of H- β -CD complexation effect with regard to $C_{max}R$ (a) (AUCR (b) for fenebrutinib in the presence and absence of itraconazole.

is more likely associated with the rosuvastatin model (Supplementary Material).

Underprediction of transporter inhibition DDI has been reported. The discrepancy between *in vitro* and *in vivo* $K_{i,u}$ is believed to be mainly due to the uncertainties associated with the *in vitro* system and assay conditions, and translation of inhibition potency from *in vitro* to *in vivo*^{9,10}; and a scaling factor (> 10) is often used. Our observation in the current work is consistent with the findings reported by others, a much lower *in vivo* $K_{i,u}$ value needs to be used to recover the clinically observed DDI. Continued effort to understand the discrepancy between *in vitro* and *in vivo* is needed.

To further confirm the relative contribution of fenebrutinib OATP1B vs. BCRP inhibition to the total observed DDI, the PBPK model simulation in combination with the endogenous biomarker measurement was implemented. The scenario simulations were conducted by turning off the BCRP inhibition in the DDI panel. The results indicated that without BCRP inhibition by fenebrutinib, rosuvastatin C_{max} and AUC would only increase by ~ 1.6 and 1.4-fold, respectively, when co-administered with fenebrutinib. The decrease in the rosuvastatin C_{max} ratio (from 5-fold to < 2 -fold) is much more pronounced than the corresponding decrease in the rosuvastatin AUC, indicating that the main contributor to the observed DDI with rosuvastatin is gut BCRP inhibition by fenebrutinib. Furthermore, the limited involvement of OATP1B inhibition in the observed clinical DDI was confirmed by the measured level of coproporphyrin I (CP-I) and CP-III, endogenous substrates of OATP1B transporters but not the BCRP transporter, in the presence and absence of fenebrutinib. The effect of multiple doses of fenebrutinib on the plasma concentration-time profiles of CP-I and CP-III was comparable following co-administration of rosuvastatin and fenebrutinib, compared with rosuvastatin alone.³ These results indicate that the main mechanism of the observed fenebrutinib-rosuvastatin DDI was the inhibition of intestinal BCRP, rather than OATP1B, by fenebrutinib.

DISCUSSION

To characterize fenebrutinib DDI potential and recommend concomitant medication strategy, a PBPK model-informed drug development strategy was implemented. An integrated approach using PBPK simulations and endogenous biomarker measurements enabled a better mechanistic understanding of fenebrutinib-rosuvastatin clinical DDI involving multiple transporters. The hypothesis-driven analysis using a mechanistic absorption PBPK model supported by *in vitro* and nonclinical *in vivo* data provided a sound rationale for the observed DDI between fenebrutinib and itraconazole with and without accounting for the effect of H- β -CD-fenebrutinib complexation. The deconvolution of the observed DDI data using mechanistic PBPK modeling, together with other clinical and nonclinical data, allowed confirmation of relative contribution of transporter inhibition by fenebrutinib as well as determination of $f_{m,CYP3A}$ in fenebrutinib clearance, without requiring additional clinical DDI studies.

Available data from nonclinical and clinical studies support that CYP3A is a major enzyme responsible for hepatic clearance, and the metabolic pathway accounting for $> 90\%$ of fenebrutinib elimination. Therefore, the observed DDI for fenebrutinib in the presence of strong CYP3A inhibitor itraconazole, specifically the absence of an increase in fenebrutinib C_{max} (observed in 12 of 14 subjects in the clinical study) could not be explained without considering other mechanisms that could reduce fenebrutinib exposure in the presence of itraconazole. Various hypotheses have been considered and tested via PBPK modeling to attempt to explain the observed C_{max} decrease, including fenebrutinib CYP3A gut metabolism, fenebrutinib interacting concentration in the gut, itraconazole and hydroxy-itraconazole concentrations in the DDI study, and inhibition of P-gp by itraconazole. The outcome of these evaluations showed that none of these hypothesis-driven PBPK simulations could explain the observed DDI data in which fenebrutinib C_{max} decreased and AUC increased in the presence of

itraconazole. For example, the exposure of itraconazole and hydroxy-itraconazole measured in the DDI study was consistent with published data,^{11,12} and the concentration-time profiles of both itraconazole and hydroxy-itraconazole PK (including accumulation after multiple doses) were well-captured by the PBPK model in the DDI simulation (**Figure S3**). In addition, inhibition of P-gp by itraconazole would only increase the C_{\max} of fenebrutinib (a less sensitive P-gp substrate), rather than decrease it.

Previous works indicated that while cyclodextrin is used as an excipient to increase solubility of a drug, it can also decrease the concentration of free drug available to permeate the intestinal membrane, due to the formation of complex between a drug and cyclodextrin.^{13–15} Further, high concentrations of cyclodextrin can reduce a drug's apparent permeability and *in situ* rat jejunal effective permeability, leading to longer T_{\max} and reduced C_{\max} , thus resulting in decreased bioavailability in rats.⁸ In the fenebrutinib DDI study with itraconazole, fenebrutinib was exposed to H- β -CD introduced from the itraconazole solution (~ 8 g of H- β -CD/dose of itraconazole). The *in vitro* study confirmed the strong molecular complexation between fenebrutinib and H- β -CD (evidenced by a high complex constant, K_{complex}) and reduced apparent permeability, and an *in vivo* dog PK showed decreased rate and extent of fenebrutinib absorption when co-administered with H- β -CD. These observations are consistent with existing knowledge, and support our approach of incorporating the hypothesis into PBPK model to explain the observed DDI between itraconazole and fenebrutinib.

To further quantitatively describe the H- β -CD effect on fenebrutinib PK, we explored the recently developed Simcyp's cyclodextrin binding model (version 18.2) that correlates the reduction of P_{eff} (predicted by MechPeff model) with a decreased unbound fraction of a drug in the presence of cyclodextrin along the GI tract. With the input parameters of high K_{complex} ($2.7 \times 10^4 \text{ M}^{-1}$) for fenebrutinib with H- β -CD (estimated from *in vitro* experiment) and the amount of H- β -CD (8 g) administered (with itraconazole solution in the DDI study), fenebrutinib PK in the presence of H- β -CD was simulated using the cyclodextrin binding model that mechanistically accounted for the H- β -CD effect on P_{eff} . **Figure S4** shows that a decrease in fenebrutinib absorption (by ~ 48%) was predicted, with decreases in C_{\max} and AUC by ~ 3.5-fold and 2.0-fold, respectively, and a delay in T_{\max} by ~ 1 hour, which is comparable to the simulated H- β -CD effect on fenebrutinib PK using the MechPeff model with manually reduced P_{eff} (model 2). Unfortunately, to simulate the effect of H- β -CD on fenebrutinib PK using cyclodextrin binding model, cyclodextrin needs to be in the inhibitor position, therefore, the simulation of itraconazole–fenebrutinib DDI cannot be conducted at the same time (because itraconazole and OH-itraconazole both need to be in inhibitor positions). To inform parameterization of H- β -CD effect for future predictions of other drugs, it will be more effective to simulate the dynamic interaction among substrate, itraconazole, and H- β -CD using a further developed model.

The $f_{\text{m,CYP3A}}$ estimate is a key parameter that enables the use of the fenebrutinib PBPK model for DDI prediction with other CYP3A inhibitors and inducers. All available

nonclinical and clinical data were used in support of $f_{\text{m,CYP3A}}$ determination and verification, including: (i) retrospective PBPK simulation of the observed DDI between fenebrutinib and itraconazole, including sensitivity analyses; (ii) human mass balance study results confirming the major clearance pathway by metabolism ($f_{\text{m}} > 90\%$); (iii) *in vitro* phenotyping data indicating CYP3A as the primary metabolizing enzyme for fenebrutinib; and (iv) multiple-dose fenebrutinib PK data with accumulation caused by auto-inhibition of CYP3A, which is captured well by PBPK simulation at the estimated $f_{\text{m,CYP3A}}$. The totality of evidence supports the classification of fenebrutinib as a sensitive CYP3A substrate, and the results of the integrated analyses suggest that fenebrutinib has an $f_{\text{m,CYP3A}}$ value ≥ 0.8 . The consistency of the data analysis provided confidence that the current PBPK model can be used to predict DDIs between fenebrutinib and other CYP3A perpetrators.

From a clinical risk perspective, the estimate of $f_{\text{m,CYP3A}}$ 0.8–0.85 likely represents the worst case DDI scenario for fenebrutinib when co-administered with a strong CYP3A inhibitor, such as itraconazole ($C_{\max,R} \sim 2.4$ and AUCR ~ 5.0). The exclusion of strong CYP3A perpetrators would likely be recommended if warranted by the therapeutic window of fenebrutinib, regardless of whether fenebrutinib is considered a sensitive or a moderately sensitive CYP3A substrate (e.g., $f_{\text{m,CYP3A}}$ 0.6 or 0.8–0.85). However, in the presence of moderate CYP3A inhibitors, dose adjustment (if needed) could be similar under these two scenarios (i.e., $f_{\text{m,CYP3A}}$ 0.6 or 0.8), because the difference in the magnitude of DDI with moderate inhibitors is much less pronounced (**Table S3**).

In conclusion, the results from our combined approach confirmed that the observed clinical DDI between fenebrutinib and rosuvastatin is primarily due to the inhibition of intestinal BCRP rather than hepatic OATP1B, which supports the proposal to use the PBPK prediction with endogenous biomarker measurements to inform recommendations around the concomitant use of fenebrutinib with other OATP1B substrates. Mechanistic PBPK modeling based on sound scientific rationale explained the clinically observed DDI between fenebrutinib and itraconazole. The totality of the evidence from PBPK sensitivity analysis and nonclinical and clinical data indicated that fenebrutinib is likely a sensitive CYP3A substrate. The consistency of the model-based analyses and the accumulated *in vitro* and *in vivo* data qualifies the PBPK model for subsequent predictions of untested scenarios for DDI between fenebrutinib and other CYP3A inhibitors and inducers.

Supporting Information. Supplementary information accompanies this paper on the *CPT: Pharmacometrics & Systems Pharmacology* website (www.psp-journal.com).

Acknowledgments. The authors thank Christine Bowman, Lin Pan, and Marcel Hop for sharing their knowledge and contributions to the valuable discussion.

Funding. No funding was received for this work.

Conflict of Interest. All authors declared no competing interests for this work.

Author Contributions. Y.C., F.M., N.J., K.Y., T.C., M.D., M.W., J.Y.J., and L.C. wrote the manuscript. Y.C., F.M., and L.C. designed the research. Y.C., F.M., N.J., T.C., M.D., and L.C. performed the research. Y.C., F.M., N.J., K.Y., T.C., M.D., and L.C. analyzed the data.

1. Crawford, J.J. *et al.* Discovery of GDC-0853: a potent, selective, and noncovalent Bruton's tyrosine kinase inhibitor in early clinical development. *J. Med. Chem.* **61**, 2227–2245 (2018).
2. Herman, A.E. *et al.* Safety, pharmacokinetics, and pharmacodynamics in healthy volunteers treated with GDC-0853, a selective reversible Bruton's tyrosine kinase inhibitor. *Clin. Pharmacol. Ther.* **103**, 1020–1028 (2018).
3. Jones, N.S. *et al.* Complex DDI by fenebrutinib and the use of transporter endogenous biomarkers to elucidate the mechanism of DDI. *Clin. Pharmacol. Ther.* **107**, 269–277 (2020).
4. Rodgers, T. & Rowland, M. Physiologically based pharmacokinetic modelling 2: predicting the tissue distribution of acids, very weak bases, neutrals and zwitterions. *J. Pharm. Sci.* **95**, 1238–1257 (2006).
5. Rowland Yeo, K., Jamei, M., Yang, J., Tucker, G.T. & Rostami-Hodjegan, A. Physiologically based mechanistic modelling to predict complex drug-drug interactions involving simultaneous competitive and time-dependent enzyme inhibition by parent compound and its metabolite in both liver and gut - the effect of diltiazem on the time-course of exposure to triazolam. *Eur. J. Pharm. Sci.* **39**, 298–309 (2010).
6. Chen, Y. *et al.* Development of a physiologically based pharmacokinetic model for itraconazole pharmacokinetics and drug-drug interaction prediction. *Clin. Pharmacokinet.* **55**, 735–749 (2016).
7. Austin, R.P., Barton, P., Cockcroft, S.L., Wenlock, M.C. & Riley, R.J. The influence of nonspecific microsomal binding on apparent intrinsic clearance, and its prediction from physicochemical properties. *Drug Metab. Dispos.* **30**, 1497–1503 (2002).
8. Dahan, A., Miller, J.M., Hoffman, A., Amidon, G.E. & Amidon, G.L. The solubility-permeability interplay in using cyclodextrins as pharmaceutical solubilizers: mechanistic modeling and application to progesterone. *J. Pharm. Sci.* **99**, 2739–2749 (2010).
9. Duan, P., Zhao, P. & Zhang, L. Physiologically based pharmacokinetic (PBPK) modeling of pitavastatin and atorvastatin to predict drug-drug interactions (DDIs). *Eur. J. Drug Metab. Pharmacokinet.* **42**, 689–705 (2017).
10. Taskar, K. *et al.* PBPK models for evaluating membrane transporter mediated DDIs: Current capabilities, case studies, future opportunities and recommendations. *Clin. Pharmacol. Ther.* **107**, 1082–1115 (2019).
11. Barone, J.A. *et al.* Enhanced bioavailability of itraconazole in hydroxypropyl-beta-cyclodextrin solution versus capsules in healthy volunteers. *Antimicrob. Agents Chemother.* **42**, 1862–1865 (1998).
12. Barone, J.A. *et al.* Food interaction and steady-state pharmacokinetics of itraconazole oral solution in healthy volunteers. *Pharmacotherapy* **18**, 295–301 (1998).
13. Rao, V.M. & Stella, V.J. When can cyclodextrins be considered for solubilization purposes? *J. Pharm. Sci.* **92**, 927–932 (2003).
14. Loftsson, T., Jarho, P., Masson, M. & Jarvinen, T. Cyclodextrins in drug delivery. *Expert Opin. Drug Deliv.* **2**, 335–351 (2005).
15. Loftsson, T., Vogensen, S.B., Brewster, M.E. & Konradsdottir, F. Effects of cyclodextrins on drug delivery through biological membranes. *J. Pharm. Sci.* **96**, 2532–2546 (2007).

© 2020 The Authors. *CPT: Pharmacometrics & Systems Pharmacology* published by Wiley Periodicals LLC on behalf of the American Society for Clinical Pharmacology and Therapeutics. This is an open access article under the terms of the Creative Commons Attribution-NonCommercial License, which permits use, distribution and reproduction in any medium, provided the original work is properly cited and is not used for commercial purposes.